

Article

## Aggregation Enhanced Responsiveness of Rationally Designed Probes to Hydrogen Sulfide for Targeted Cancer Imaging

Rongchen Wang, Xianfeng Gu, Qizhao Li, Jie Gao, Ben Shi, Ge Xu, Tianli Zhu, He Tian, and Chunchang Zhao

*J. Am. Chem. Soc.*, **Just Accepted Manuscript** • DOI: 10.1021/jacs.0c06533 • Publication Date (Web): 29 Jul 2020

Downloaded from pubs.acs.org on August 2, 2020

### Just Accepted

“Just Accepted” manuscripts have been peer-reviewed and accepted for publication. They are posted online prior to technical editing, formatting for publication and author proofing. The American Chemical Society provides “Just Accepted” as a service to the research community to expedite the dissemination of scientific material as soon as possible after acceptance. “Just Accepted” manuscripts appear in full in PDF format accompanied by an HTML abstract. “Just Accepted” manuscripts have been fully peer reviewed, but should not be considered the official version of record. They are citable by the Digital Object Identifier (DOI®). “Just Accepted” is an optional service offered to authors. Therefore, the “Just Accepted” Web site may not include all articles that will be published in the journal. After a manuscript is technically edited and formatted, it will be removed from the “Just Accepted” Web site and published as an ASAP article. Note that technical editing may introduce minor changes to the manuscript text and/or graphics which could affect content, and all legal disclaimers and ethical guidelines that apply to the journal pertain. ACS cannot be held responsible for errors or consequences arising from the use of information contained in these “Just Accepted” manuscripts.

# Aggregation Enhanced Responsiveness of Rationally Designed Probes to Hydrogen Sulfide for Targeted Cancer Imaging

Rongchen Wang,<sup>†,§</sup> Xianfeng Gu,<sup>‡,§</sup> Qizhao Li,<sup>†</sup> Jie Gao,<sup>‡</sup> Ben Shi,<sup>†</sup> Ge Xu,<sup>†</sup> Tianli Zhu,<sup>†</sup> He Tian,<sup>†</sup> Chunchang Zhao<sup>\*,†</sup>

<sup>†</sup> Key Laboratory for Advanced Materials and Feringa Nobel Prize Scientist Joint Research Center, Institute of Fine Chemicals, School of Chemistry and Molecular Engineering, East China University of Science and Technology, Shanghai, 200237, P. R. China.

<sup>‡</sup> Department of Medicinal Chemistry, School of Pharmacy, Fudan University, Shanghai, 201203, P. R. China.

**ABSTRACT:** Activatable molecular probes hold great promise for targeted cancer imaging. However, the hydrophobic nature of most conventional probes makes them generate precipitated agglomerate in aqueous media, thereby annihilating their responsiveness to analytes and precluding their practical applications for bioimaging. This study reports the development of two small molecular probes with unprecedented aggregation enhanced responsiveness to H<sub>2</sub>S for in vivo imaging of H<sub>2</sub>S-rich cancers. The subtle modulation of the equilibrium between hydrophilicity and lipophilicity by N-ethylpyridinium endows these designed probes with the capability of spontaneously self-assembling into nanoprobe under physiological conditions. Such probes in an aggregated state, rather than a molecular dissolved state, show NIR fluorescence light up and photoacoustic signals turn on upon H<sub>2</sub>S specific activation, allowing in vivo visualization and differentiation of cancers based on differences in H<sub>2</sub>S content. Thus, our study presents an effective design strategy which should pave the way to molecular design of optimized probes for precision cancer diagnostics.

## INTRODUCTION

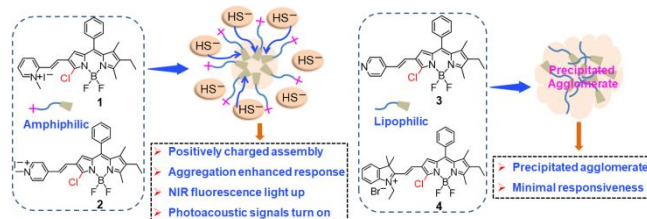
Activatable molecular probes that change fluorescent signals only in response to cancer-related biomarkers greatly facilitate the advancement of targeted cancer imaging.<sup>1-3</sup> In this context, various activatable fluorescent probes capable of detection of diverse molecular targets in cancers have been successfully developed over the years.<sup>4-20</sup> The prerequisite of a practical system for in vivo imaging is the capability of a molecular probe to function well under physiological conditions. Although a large number of activatable small molecule probes are now available, they naturally tend to aggregate into precipitated agglomerate in aqueous media due to the hydrophobic nature of most conventional organic probes; this results in minimal responsiveness to analytes.<sup>21-26</sup> Such characteristics preclude their practical applications for bioimaging.

Because increased H<sub>2</sub>S production gives rise to tumorigenesis in many cancers, H<sub>2</sub>S-activatable molecular probes should unambiguously provide valuable insight into precise cancer imaging.<sup>27-32</sup> However, the use of H<sub>2</sub>S-responsive probes for cancer imaging is still in its infancy. Although many H<sub>2</sub>S-responsive fluorescent probes have been established and found widespread applications,<sup>33-41</sup> most of them are inapplicable for in vivo tumor location presumably due to several intrinsic drawbacks including poor hydrophilicity and slow reaction with H<sub>2</sub>S in aqueous solution. To address these issues, great efforts have been devoted to engineering water-soluble nanoprobe through encapsulation of small activatable molecule probes into the hydrophobic interiors of nanocomposites.<sup>42-46</sup> These devised nanoprobe realize accurate identification of cancers by real-time trapping

of endogenous H<sub>2</sub>S. Despite the advances, these nanoprobe are still subject to the limitations of complicated fabrication processes and poor preparation reproducibility, which is not conducive to clinical translation. Therefore, it is of great scientific interest to develop new activatable small molecules that are capable of spontaneous self-assembly to form monodisperse nanoparticles with improved optical responsiveness for cancer imaging.

Herein, we report two small molecular probes that show unprecedented aggregation enhanced responsiveness (AER) to H<sub>2</sub>S for in vivo imaging of H<sub>2</sub>S-rich cancers. Our designed molecules are shown in [Scheme 1](#), in which the hydrophilic N-ethylpyridinium acts as the electron withdrawing group, while the hydrophobic monochlorinated BODIPY core acts as the H<sub>2</sub>S-responsive unit. Different from the traditional lipophilic molecular probes (e.g. probes 3 and 4), which always have poor or no response to analytes in pure aqueous solutions because of their limited water solubility and the resultant precipitation tendencies under physiological conditions,<sup>21-24</sup> the designed amphiphilic probes 1 and 2 were able to spontaneously self-assemble into nanoprobe with well-defined nanostructure and showed surprising aggregation enhanced responsiveness to H<sub>2</sub>S in buffers. High absorption bands within NIR regions were activated upon introduction of H<sub>2</sub>S, which gave rise to bright NIR emissions lighting up in assembled 1 (the assembled form of probe 1) and strong photoacoustic signals turning on in assembled 2 (the assembled form of probe 2). However, the molecularly dissolved probe 1 and 2 in the bulk solutions gave minimal optical changes upon introduction of H<sub>2</sub>S. Undoubtedly, as compared to traditional activatable probes, the unprecedented

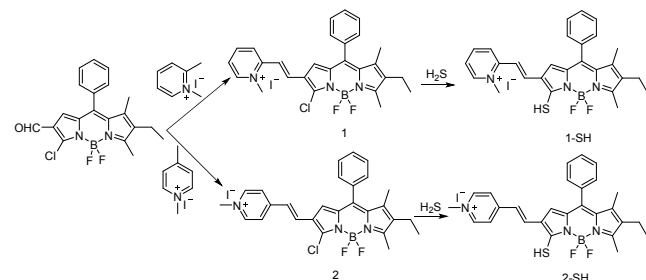
aggregation enhanced responsiveness makes probes 1 and 2 ideal candidates for biosensing and imaging *in vivo*. As a proof-of-concept example, using the assembled 1 that emitted NIR fluorescence at 718 nm upon H<sub>2</sub>S activation, accurate identification and differentiation of cancers were realized by real-time trapping of endogenous H<sub>2</sub>S. This is the first example in which a small molecular probe shows spontaneous self-assembly in an aqueous medium with greatly enhanced responsiveness to analytes, thus paving the way to molecular design of optimized probes for precision cancer diagnostics.



Scheme 1. Chemical structures of 1, 2, 3, and 4. The amphiphilic nature of 1 and 2 leads to spontaneous formation of positively charged assemblies, while the lipophilic 3 and 4 forms precipitated agglomerate in aqueous media. Such disparity endows the probes with distinct responsiveness to H<sub>2</sub>S under physiological conditions.

## RESULTS AND DISCUSSION

As presented in Scheme 2 and Scheme S1, probes 1 and 2 were readily synthesized by the Knoevenagel condensation of a known aldehyde BODIPY<sup>47</sup> with 2-methyl-N-ethylpyridinium and 4-methyl-N-ethylpyridinium, respectively. The control probes 3 and 4 were prepared following the similar synthesis procedure, wherein 4-methylenepyridine and N-ethyl-2,3,3-trimethylindolenine were linked to BODIPY core to elongate the conjugated system. <sup>1</sup>H and <sup>13</sup>C NMR spectroscopy and HRMS identified their structures and their high purity.



Scheme 2. Synthesis procedure and proposed S<sub>N</sub>Ar reaction of probe 1 and 2 with H<sub>2</sub>S.

Interestingly, the optical response of probes 1 and 2 to H<sub>2</sub>S heavily depended on the volume fraction of water (fw) in the CH<sub>3</sub>CN/Tris mixtures (pH 7.4, room temperature). For example, the molecular dissolved probe 1 with 2-methylene-N-ethylpyridinium function gave poor optical changes upon introduction of 100 μM NaHS at fw = 50%. However, as the fw value gradually increased from 50% to 90%, the H<sub>2</sub>S-activated new absorption enhanced significantly and the absorption peak hypsochromically shifted from 659 nm to 644 nm (Figure 1a and Figure S1). Similarly, the H<sub>2</sub>S-activated NIR emission increased sharply and the emission peak shifted from 751 to 725 nm upon increasing fw from 50% to 90% (Figure 1b). These H<sub>2</sub>S-initiated optical features upon increasing fw were ascribed to the aggregation enhanced

conversion of probe 1 to 1-SH via thiol-halogen nucleophilic aromatic substitution reaction (S<sub>N</sub>Ar) (Scheme 2 and Figure S2). The native fluorescent features of 1 and 1-SH (fluorescence quantum yield = 0.88% for assembled state in pure Tris buffer) afford no contributions to such aggregation enhanced NIR emission due to the fact that probe 1 and 1-SH show aggregation caused fluorescence quenching properties (Table S1 and Figure S3).

Notably, after reaching the best performance at fw = 90%, both the absorption and fluorescence responsiveness was slightly attenuated upon further increasing the water fraction fw. Nevertheless, self-assembled probe 1 produced highly efficient responsiveness to H<sub>2</sub>S in 100% buffer, thus indicating its suitability for visualization of H<sub>2</sub>S in living systems. The amphiphilic probe 1 spontaneously self-assembled into nanoprobe and showed aggregation enhanced responsiveness to H<sub>2</sub>S in buffers. This unprecedented AER was further confirmed by the pseudo-first-order kinetics (k<sub>obs</sub>) at various fw. As expected (Figure S4), assembled 1 at fw = 100% exhibited much faster k<sub>obs</sub> (7.13 × 10<sup>-3</sup> S<sup>-1</sup>) than that of molecular dissolved 1 at fw = 50% (2.81 × 10<sup>-3</sup> S<sup>-1</sup>).

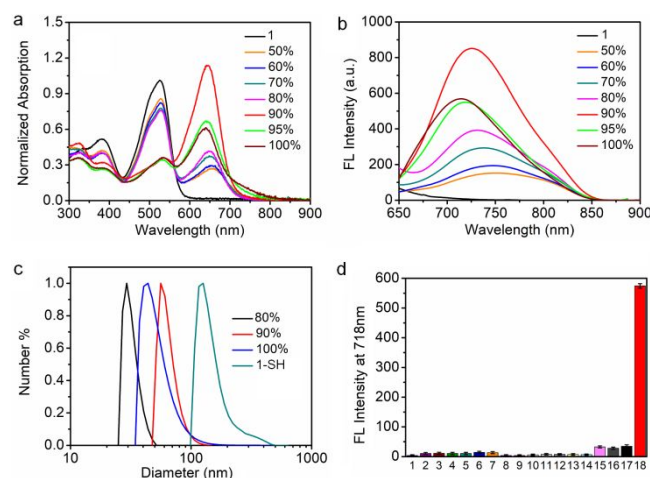


Figure 1. Normalized absorption (a) and fluorescence (b) responses of probe 1 (10 μM) to NaHS (100 μM) in CH<sub>3</sub>CN/Tris mixtures with various fw. Data were recorded 60 min after addition of NaHS. Line 1 (black line) represents the absorption and fluorescence of probe 1 without H<sub>2</sub>S. (c) DLS size profiles of assembled 1 (10 μM) at various fw. Line 1-SH indicates the size of assembled 1-SH at fw = 100%. (d) Fluorescence intensity changes of assembled 1 upon addition of NaHS (100 μM) and other competing analytes (1 mM) in Tris buffer (pH 7.4). 1) Free; 2) F<sup>-</sup>; 3) Cl<sup>-</sup>; 4) Br<sup>-</sup>; 5) I<sup>-</sup>; 6) NO<sub>2</sub><sup>-</sup>; 7) N<sub>3</sub><sup>-</sup>; 8) HCO<sub>3</sub><sup>-</sup>; 9) SO<sub>4</sub><sup>2-</sup>; 10) HPO<sub>4</sub><sup>2-</sup>; 11) ClO<sup>-</sup>; 12) H<sub>2</sub>O<sub>2</sub>; 13) OAc<sup>-</sup>; 14) S<sub>2</sub>O<sub>3</sub><sup>2-</sup>; 15) GSH; 16) Hcy; 17) Cys; 18) NaHS. Data were recorded 60 min after addition of NaHS.

The aggregate formation of probe 1 could be confirmed by dynamic light scattering (DLS) measurements (Figure 1c). At fw = 50%, 60% and 70 %, probe 1 was found to be in the molecularly dissolved state in CH<sub>3</sub>CN/Tris buffer mixtures; thus, no DLS signals were detectable. However, probe 1 was prone to form aggregates with average diameter of 29 ± 4 nm at fw = 80%, 56 ± 5 nm at fw = 90% and 43 ± 5 nm at fw = 100%. Additional characterizations of the corresponding morphology were also performed by scanning electron microscopy (SEM) (Figure S5). Notably, assembled 1-SH aggregated into much larger particles (124 ± 13 nm) at fw =

100%, enabling a long residence time in the target cells to achieve high imaging contrast.<sup>48-49</sup> More importantly, both assembled 1 and assembled 1-SH had good stability in buffers (Figure S6).

In 100% Tris buffer, the fluorescence intensity of assembled 1 showed good linear correlation within the H<sub>2</sub>S concentration range from 0 to 30 μM (Figure S7), thus affording a detection limit of 60 nM which shows that assembled 1 could provide sensitive detection of H<sub>2</sub>S. It was also found that assembled 1 exhibited a highly selective response to H<sub>2</sub>S. A distinct enhancement of the fluorescence intensity at 718 nm was triggered by H<sub>2</sub>S and not by other interfering species (Figure 1d and Figure S8). Importantly, such distinct responsiveness of assembled 1 to H<sub>2</sub>S was maintained in a cell culture medium (Figure S9), indicative of no interference from biological contexts. Of note, assembled 1 was readily activated to give good optical response within a physiological pH range of 8.5 to approximately 5.5 (Figure S10).

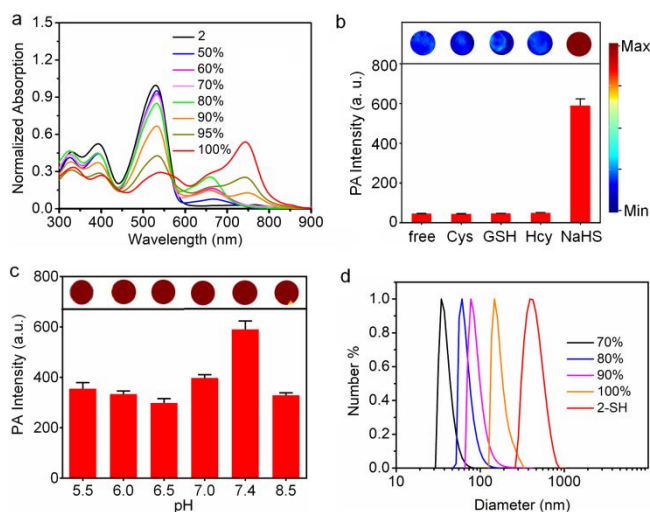


Figure 2. (a) Normalized absorption responses of probe 2 (10 μM) to NaHS (100 μM) at various fw. Data were recorded 60 min after addition of NaHS. Line 2 (black line) represents the absorption of probe 2 without NaHS. (b) Photoacoustic amplitude changes of assembled 2 (80 μM) upon addition of NaHS (100 μM) and other competing analytes (1 mM) in pure Tris buffer (pH 7.4, room temperature). Data were collected 60 min after addition of NaHS. (c) The good PA responsiveness of assembled 2 to H<sub>2</sub>S within a wide pH range. (d) DLS size profiles of assembled 2 (10 μM) at various fw. Line 2-SH indicates the size of assembled 2-SH at fw = 100%.

In the case of probe 2 with 4-methylene-N-ethylpyridinium function, its amphiphilic nature enabled 2 to readily self-assemble in physiological conditions. Owing to the aggregation, probe 2 attained enhanced optical response to H<sub>2</sub>S. Its H<sub>2</sub>S-initiated NIR absorption gradually enhanced with gradually increasing fw from 50% to 80%, and the absorption peak slightly shifted from 667 nm to 658 nm. Impressively, further increasing fw from 80% to 100%, a new absorption band around 744 nm was found to evolve sharply, accompanied by the higher energy peak around 658 nm as a shoulder (Figure 2a and Figure S11), indicative of self-assembled 2 in 100% buffer being a H<sub>2</sub>S-activatable photoacoustic probe. The H<sub>2</sub>S-initiated induction of NIR absorption at 744 nm was not interrupted by biological contexts such as a cell culture medium (Figure S9). Such an

emergence of NIR absorption at 744 nm could be ascribed to the gradual evolution of aggregates from loose to compact, which leads to a reduced energy gap between HOMO and LUMO. According to H<sub>2</sub>S-initiated NIR absorption changes, a detection limit of 760 nM was determined for assembled 2 (Figure S12).

The photoacoustic responsiveness of assembled 2 to H<sub>2</sub>S was then evaluated in buffer solutions (pH 7.4). In the absence of H<sub>2</sub>S, no detectable photoacoustic signals were initiated. In contrast, when H<sub>2</sub>S was introduced to the solution, bright photoacoustic signals were produced following excitation at 750 nm, which ultimately afforded a 13-fold turn-on response (Figure 2b). The H<sub>2</sub>S-activated PA intensities of assembled 2 showed a dose-dependent enhancement (Figure S12). This H<sub>2</sub>S-initiated strong PA signal showed no interference from 1 mM GSH and 1 mM Cys, indicative of the probe's potential for imaging applications in complex living systems. Furthermore, the good PA responsiveness to H<sub>2</sub>S was found to be retained within a physiological range from pH 8.5 to approximately 5.5 (Figure 2c).

In order to acquire insight into the self-assembly process of probe 2 that forms aggregates, the average sizes of formed nanoparticles in CH<sub>3</sub>CN/Tris buffer mixtures with different fw were monitored through DLS assay and SEM characterization. The DLS results (Figure 2d) showed that the assembled 2 has sizes of about 35 ± 5 nm at fw = 70%, 61 ± 8 nm at fw = 80%, 77 ± 7 nm at fw = 90% and 148 ± 12 nm at fw = 100%. No DLS signals, however, could be obtained from the solution at fw = 50% and 60% due to the fact that probe 2 is in the molecularly dissolved state in these solutions. In addition, it was found that assembled 2 and assembled 2-SH showed good stability in buffers (Figure S13).

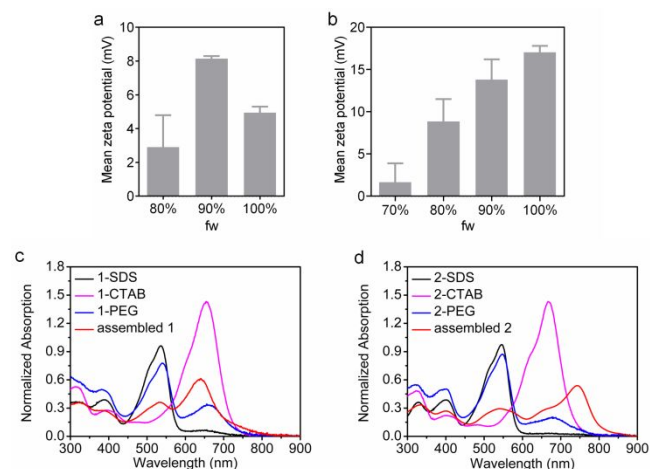


Figure 3. (a) Mean zeta potential of probe 1 (10 μM) at various fw. (b) Mean zeta potential of probe 2 (10 μM) at various fw. (c) Normalized absorption responses of 1-SDS, 1-CTAB, 1-PEG, and assembled 1 (probe 1, 10 μM) to NaHS (100 μM). (d) Normalized absorption responses of 2-SDS, 2-CTAB, 2-PEG, and assembled 2 (probe 2, 10 μM) to NaHS (100 μM).

The aforementioned unprecedented aggregation enhanced responsiveness of probe 1 and 2 could be ascribed to an important concern: the self-assembly of probe 1 and 2 in aqueous solution affords aggregations with enhanced positive charge density that enriches the local concentrations of HS<sup>-</sup> (main forms of H<sub>2</sub>S in physiological pH) close to

monochlorinated BODIPY,<sup>50-52</sup> thus facilitating the  $S_NAr$  reaction. In contrast, the molecularly dissolved state of probes 1 and 2 in the bulk solutions had minimal  $H_2S$  enrichment effect, thus resulting in poor responsiveness. The mean zeta potential values of assembled probes in  $CH_3CN/Tris$  buffer mixtures with different fw stayed highly consistent with the observed responsiveness to  $H_2S$  (Figure 3a and Figure 3b), inferring that positive charge density played a vital role in regulating the reaction of the probes with  $H_2S$ .

To elucidate the essential role of positive charge in accelerating the responsive performance, we further established nanoprobe 1/2-SDS, 1/2-CTAB and 1/2-PEG via encapsulating probe 1 or 2 into the hydrophobic interiors of micelles based on sodium dodecylsulfonate (SDS, anionic surfactant), cetyltriethylammonium bromide (CTAB, cationic surfactant), and amphiphilic copolymer (mPEG-DSPE), respectively. Experimental data showed that the highly positive charged nature of 1/2-CTAB led to markedly rapid optical responses to  $H_2S$  in approximately 2 min, accompanied by enhanced optical changes (Figure 3c-d and Figure S14-15). In sharp contrast, 1/2-SDS gave minimal optical changes in approximately 120 min since the negatively charged surface prevented anion  $HS^-$  from accessing probes 1 and 2 within the hydrophobic cores. Interestingly, because of the neutral nature of 1/2-PEG, mild responsiveness was observed. Within these nanoprobe, small molecular probes 1 and 2 were maintained at low local concentrations to minimize aggregation processes in micelles.<sup>36</sup> Accordingly, no aggregation induced red-shift of the absorption of 2-SH to 744 nm was observed in 2-CTAB and 2-PEG. The specific generation of NIR absorption at 744 nm thus indicated the superiority of self-assembled 2 as an activatable photoacoustic probe.

To further demonstrate the vital role of the positive charge on the enrichment of  $HS^-$  for inducing and accelerating the responsiveness, probe 3 was synthesized; it had pyridine rather than N-ethylpyridinium appending to the BODIPY core through a vinylene unit. Since probe 3 had no cation function and is lipophilic, this probe formed agglomerates that precipitated in buffer. In consequence, negligible  $H_2S$ -activated absorption and emission could be observed with increasing fw from 50% to 100% (Figure S16), indicative of no aggregation enhanced responsiveness effect. We previously reported an  $H_2S$ -activatable probe 4,<sup>36</sup> wherein electron-withdrawing N-ethyl-2,3,3-trimethylindolenine was appended to the BODIPY core through a vinylene unit. As indolium is a lipophilic cation in nature, probe 4 naturally produces precipitated agglomerates in aqueous media. Consequently, probe 4 possessed good  $H_2S$ -activated performance when it was well dissolved in  $CH_3CN/Tris$  media with fw = 50% (Figure S17). In contrast, minimal optical changes were initiated by  $H_2S$  at fw = 100%. Evidently, probe 4 exhibited an opposite performance compared to probe 1 and 2. Hence the subtle variation of electron withdrawing groups appending to monochlorinated BODIPY can generate great differences in hydrophilicity and optical responsiveness to  $H_2S$  under physiological conditions. Undoubtedly, as compared to traditional activatable probes, the unprecedented aggregation enhanced responsiveness makes probes 1 and 2 good candidates for biosensing and imaging in vivo.

The widely available instruments for NIR fluorescence imaging and activatable fluorescent probes are valuable tools in medicine,<sup>53-55</sup> so we used assembled 1 as a proof-of-concept

model probe to further explore the potential applications in living systems. To identify and differentiate cancer cells, fluorescence light up imaging was performed with  $H_2S$ -rich HCT116 cells and  $H_2S$ -deficient HepG2 cells. After demonstration of a high biocompatibility in living cells (Figure S18), cell imaging experiments were subsequently conducted. As shown in Figure 4a, the incubation of HCT116 cells with assembled 1 for 1 h afforded bright red fluorescence signals. To clarify that the obtained red fluorescence signal was indeed activated by endogenous  $H_2S$ , inhibitor and activator assays were performed. The inhibitory production of cellular  $H_2S$  by cystathionine- $\beta$ -synthase (CBS) inhibitor aminooxyacetic acid (AOAA) attenuated the red fluorescence in HCT116 cells, while the promotion of  $H_2S$  production by allosteric CBS activator S-adenosyl-l-methionine (SAM) resulted in an increase of the red fluorescence. Due to the  $H_2S$ -deficiency in HepG2 cells, treatment of these living cells with assembled 1 revealed no detectable red fluorescence signals (Figure 4b). Furthermore, pretreatment of HepG2 cells with AOAA or SAM also induced minimal red fluorescence images. Collectively, assembled 1 can be used to selectively image  $H_2S$ -rich cancer cells by tracking endogenous  $H_2S$  and differentiate types of living cells based on  $H_2S$  contents (rich vs deficient). Also, we successfully established the applicability of assembled 1 for tracking endogenous  $H_2S$  production by performing experiments with raw264.7 macrophages and Cardiomyocytes cells that express the  $H_2S$ -producing enzyme cystathionine  $\gamma$ -lyase (CSE) (Figure S19 and S20). Additionally, the spot-like cell images presented a direct observation of the aggregation of probe 1 in cells (Figure S21).<sup>56</sup>

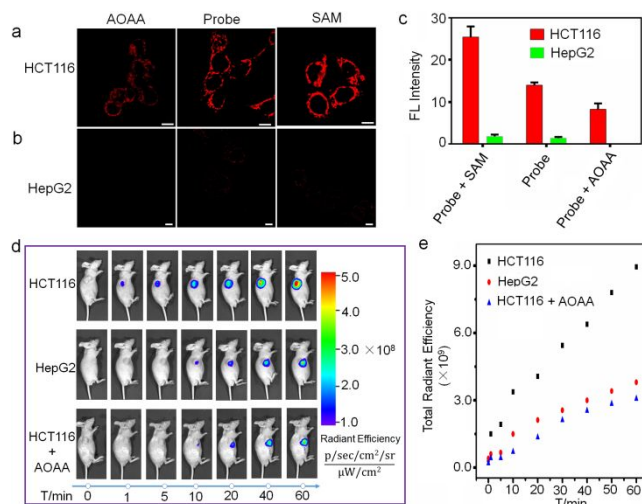


Figure 4. Identification and differentiation of  $H_2S$ -rich HCT116 cells (a) and  $H_2S$ -deficient HepG2 cells (b) after incubation with assembled 1 at 37 °C for 1 h. Inhibitor and activator assay were performed by pretreatment of cells with AOAA (1 mM) and SAM (3 mM), followed by further incubation with assembled 1 for 1h. Scale bar = 10  $\mu m$ . (c) Relative fluorescence intensities quantified from images in (a) and (b). (d) Representative fluorescence images of tumor-bearing mice at different time post subcutaneous injection of assembled 1 (30 nmol) into tumor-bearing mouse models for identification and differentiation of cancers based on  $H_2S$ -specific activation. (e) Fluorescence intensities of tumors quantified from images in (d).

Next, assembled 1 was further explored to identify and differentiate types of cancers based on  $H_2S$  contents through

subcutaneous injection into H<sub>2</sub>S-rich HCT116 tumor-bearing mouse models and H<sub>2</sub>S-deficient HepG2 tumor-bearing mouse models (Figure 4). The NIR fluorescence images of H<sub>2</sub>S-rich HCT116 tumor indicated that obvious NIR emission was initiated within 1 min post-injection of assembled 1, indicative of rapid activation in H<sub>2</sub>S-rich regions. This fluorescence intensity gradually increased over time and leveled off at 60 min post-injection. The HCT116 tumor visualization based on H<sub>2</sub>S-activation of assembled 1 was further confirmed by in vivo inhibition assay. It was found that attenuation of NIR fluorescence emerged when the HCT 116 tumor was pretreated by AOAA. Note that at 1 h after injection, the NIR fluorescence signal in the HCT 116 tumor region was triple that in AOAA-pretreated tumors. Owing to the low level of H<sub>2</sub>S in HepG2 tumors, the NIR fluorescence signals slightly increased (Figure 4d), and thus it was hard to delineate the tumor. These imaging data demonstrated that the increased NIR fluorescence signals in the tumor region came from H<sub>2</sub>S-specific activation of assembled 1, which enables the discrimination of H<sub>2</sub>S-rich cancers from those that possess low H<sub>2</sub>S level.

## CONCLUSION

In summary, we designed and synthesized two small molecular probes that possess unprecedented aggregation enhanced responsiveness to H<sub>2</sub>S for in vivo imaging of H<sub>2</sub>S-rich cancers. Traditional activatable molecular probes readily aggregate to precipitated agglomerates in aqueous media and, in that form, provide minimal responsiveness to analytes. In contrast, our designed probes displayed H<sub>2</sub>S specific activation in the aggregated state rather than in the molecularly dissolved state, giving rise to bright NIR emissions lighting up and strong photoacoustic signals turning on responses which make these new probes ideal candidates for in vivo imaging. Such unique characteristics allow identifying and differentiating types of cancers based on H<sub>2</sub>S contents. The new probes are the first examples that show aggregation enhanced responsiveness to analytes in an aqueous medium. This work presents a promising approach to the design of optimized probes for precisely targeted cancer imaging.

## ASSOCIATED CONTENT

**Supporting Information.** Detailed synthesis and experimental procedures, supplementary figures, and characterizations are provided. This material is available free of charge via the Internet at <http://pubs.acs.org>.

## AUTHOR INFORMATION

### Corresponding Author

\* E-mail: zhaocchang@ecust.edu.cn

### Author Contributions

R. W., X. G. contributed equally.

### Notes

The authors declare no competing financial interest.

## ACKNOWLEDGMENT

We gratefully acknowledge financial support by the National Natural Science Foundation of China (21672062, 21874043, 21572039, 21788102) and Shanghai Municipal Science and Technology Major Project (Grant No.2018SHZDZX03).

## REFERENCES

- Zhang, J.; Chai, X.; He, X.-P.; Kim, H.-J.; Yoon, J.; Tian, H. Fluorogenic probes for disease-relevant enzymes. *Chem. Soc. Rev.* **2019**, *48*, 683.
- Liu, H.-W.; Chen, L.; Xu, C.; Li, Z.; Zhang, H.; Zhang, X.-B.; Tan, W. Recent progresses in small-molecule enzymatic fluorescent probes for cancer imaging. *Chem. Soc. Rev.* **2018**, *47*, 7140.
- Razgulin, A.; Ma, N.; Rao, J. Strategies for in vivo imaging of enzyme activity: an overview and recent advances. *Chem. Soc. Rev.* **2011**, *40*, 4186.
- Wu, X.; Shi, W.; Li, X.; Ma, H. A Strategy for Specific Fluorescence Imaging of Monoamine Oxidase A in Living Cells. *Angew. Chem. Int. Ed.* **2017**, *56*, 15319.
- Chen, W.; Matsunaga, T.; Neill, D. L.; Yang, C.-T.; Akaike, T.; Xian, M. Rational Design of a Dual-Reactivity-Based Fluorescent Probe for Visualizing Intracellular HSNO. *Angew. Chem. Int. Ed.* **2019**, *58*, 16067.
- Cheng, H.-B.; Zhang, Y.-M.; Liu, Y.; Yoon, J. Turn-On Supramolecular Host-Guest Nanosystems as Theranostics for Cancer. *Chem.* **2019**, *5*, 553.
- Zhang, H.; Fan, J.; Wang, J.; Zhang, S.; Dou, B.; Peng, X. An Off-On COX-2-Specific Fluorescent Probe: Targeting the Golgi Apparatus of Cancer Cells. *J. Am. Chem. Soc.* **2013**, *135*, 11663.
- Miao, Q.; Yeo, D. C.; Wirajaja, C.; Zhang, J.; Ning, X.; Xu, C.; Pu, K. Near-Infrared Fluorescent Molecular Probe for Sensitive Imaging of Keloid. *Angew. Chem. Int. Ed.* **2018**, *57*, 1256.
- Zhou, Z.; Wang, F.; Yang, G.; Lu, C.; Nie, J.; Chen, Z.; Ren, J.; Sun, Q.; Zhao, C.; Zhu, W.-H. A Ratiometric Fluorescent Probe for Monitoring Leucine Aminopeptidase in Living Cells and Zebrafish Model. *Anal. Chem.* **2017**, *89*, 11576.
- Li, H.; Li, Y.; Yao, Q.; Fan, J.; Sun, W.; Long, S.; Shao, K.; Du, J.; Wang, J.; Peng, X. In situ imaging of aminopeptidase N activity in hepatocellular carcinoma: a migration model for tumour using an activatable two-photon NIR fluorescent probe. *Chem. Sci.* **2019**, *10*, 1619.
- Gu, K.; Xu, Y.; Li, H.; Guo, Z.; Zhu, S.; Zhu, S.; Shi, P.; James, T. D.; Tian, H.; Zhu, W.-H. Real-Time Tracking and In Vivo Visualization of  $\beta$ -Galactosidase Activity in Colorectal Tumor with a Ratiometric Near-Infrared Fluorescent Probe. *J. Am. Chem. Soc.* **2016**, *138*, 5334.
- Li, Y.; Sun, Y.; Li, J.; Su, Q.; Yuan, W.; Dai, Y.; Han, C.; Wang, Q.; Feng, W.; Li, F. Ultrasensitive Near-Infrared Fluorescence-Enhanced Probe for in Vivo Nitroreductase Imaging. *J. Am. Chem. Soc.* **2015**, *137*, 6407.
- Wang, R.; Chen, J.; Gao, J.; Chen, J.-A.; Xu, G.; Zhu, T.; Gu, X.; Guo, Z.; Zhu, W.; Zhao, C. A molecular design strategy toward enzyme-activated probes with near-infrared I and II fluorescence for targeted cancer imaging. *Chem. Sci.* **2019**, *10*, 7222.
- Zheng, X.; Wang, X.; Mao, H.; Wu, W.; Liu, B.; Jiang, X. Hypoxia-specific ultrasensitive detection of tumours and cancer cells in vivo. *Nat. Commun.* **2015**, *6*, 5834.
- Wang, F.; Zhu, Y.; Zhou, L.; Pan, L.; Cui, Z.; Fei, Q.; Luo, S.; Pan, D.; Huang, Q.; Wang, R.; Zhao, C.; Tian, H.; Fan, C. Fluorescent In Situ Targeting Probes for Rapid Imaging of Ovarian-Cancer-Specific  $\gamma$ -Glutamyltranspeptidase. *Angew. Chem. Int. Ed.* **2015**, *54*, 7349.
- Liu, Y.; Tan, J.; Zhang, Y.; Zhuang, J.; Ge, M.; Sh, B.; Li, J.; Xu, G.; Xu, S.; Fan, C.; Zhao, C. Visualizing glioma margins by real-time tracking of  $\gamma$ -glutamyltranspeptidase activity. *Biomaterials* **2018**, *173*, 1.
- Urano, Y.; Sakabe, M.; Kosaka, N.; Ogawa, M.; Mitsunaga, M.; Asanuma, D.; Kamiya, M.; Young, M. R.; Nagano, T.; Choyke, P. L. Rapid Cancer Detection by Topically Spraying a  $\gamma$ -Glutamyltranspeptidase-Activated Fluorescent Probe. *Sci. Transl. Med.* **2011**, *3*, 110ra119.
- Gu, K.; Qiu, W.; Guo, Z.; Yan, C.; Zhu, S.; Yao, D.; Shi, P.; Tian, H.; and Zhu, W.-H. An enzyme-activatable probe liberating AIEgens: on-site sensing and long-term tracking of  $\beta$ -galactosidase in ovarian cancer cells. *Chem. Sci.* **2019**, *10*, 398.

- (19) Li, X.; Kim, C.-Y.; Lee, S.; Lee, D.; Chung, H.-M.; Kim, G.; Heo, S.-H.; Kim, C.; Hong, K.-S.; Yoon, J. Nanostructured Phthalocyanine Assemblies with Protein-Driven Switchable Photoactivities for Biophotonic Imaging and Therapy. *J. Am. Chem. Soc.* **2017**, *139*, 10880.
- (20) Dong, Z.; Feng, L.; Hao, Y.; Chen, M.; Gao, M.; Chao, Y.; Zhao, H.; Zhu, W.; Liu, J.; Liang, C.; Zhang, Q.; Liu, Z. Synthesis of Hollow Biomineralized CaCO<sub>3</sub>-Polydopamine Nanoparticles for Multimodal Imaging-Guided Cancer Photodynamic Therapy with Reduced Skin Photosensitivity. *J. Am. Chem. Soc.*, **2018**, *140*, 2165.
- (21) Yuan, Y.; Zhang, C.-J.; Gao, M.; Zhang, R.; Tang, B. Z.; Liu, B. Specific Light-Up Bioprobe with Aggregation-Induced Emission and Activatable Photoactivity for the Targeted and Image-Guided Photodynamic Ablation of Cancer Cells. *Angew. Chem. Int. Ed.* **2015**, *54*, 1780.
- (22) Niu, L.-Y.; Chen, Y.-Z.; Zheng, H.-R.; Wu, L.-Z.; Tung, C.-H.; Yang, Q.-Z. Design strategies of fluorescent probes for selective detection among biothiols. *Chem. Soc. Rev.* **2015**, *44*, 6143.
- (23) Li, X.; Lee, D.; Huang, J.-D.; Yoon, J. Phthalocyanine-Assembled Nanodots as Photosensitizers for Highly Efficient Type I Photoreactions in Photodynamic Therapy. *Angew. Chem. Int. Ed.* **2018**, *57*, 9885.
- (24) Zhen, X.; Zhang, J.; Huang, J.; Xie, C.; Miao, Q.; Pu, K. Macrotheranostic Probe with Disease-Activated Near-Infrared Fluorescence, Photoacoustic, and Photothermal Signals for Imaging-Guided Therapy. *Angew. Chem. Int. Ed.* **2018**, *57*, 7804.
- (25) Peng, H.-Q.; Niu, L.-Y.; Chen, Y.-Z.; Wu, L.-Z.; Tung, C.-H.; Yang, Q.-Z. Biological Applications of Supramolecular Assemblies Designed for Excitation Energy Transfer. *Chem. Rev.* **2015**, *115*, 7502.
- (26) Feng, L.; Betzer, O.; Tao, D.; Sadan, T.; Popovtzer, R.; Liu, Z. Oxygen Nanoshuttles for Tumor Oxygenation and Enhanced Cancer Treatment. *CCS Chem.* **2019**, *1*, 239.
- (27) Ma, Y.; Li, X.; Li, A.; Yang, P.; Zhang, C.; Tang, B. H<sub>2</sub>S-Activable MOF Nanoparticle Photosensitizer for Effective Photodynamic Therapy against Cancer with Controllable Singlet-Oxygen Release. *Angew. Chem. Int. Ed.* **2017**, *56*, 13752.
- (28) Zhang, K.; Zhang, J.; Xi, Z.; Li, L.-Y.; Gu, X.; Zhang, Q.-Z.; Yi, L. A new H<sub>2</sub>S-specific near-infrared fluorescence-enhanced probe that can visualize the H<sub>2</sub>S level in colorectal cancer cells in mice. *Chem. Sci.* **2017**, *8*, 2776.
- (29) Shi, B.; Yan, Q. L.; Tang, J.; Xin, K.; Zhang, J. C.; Zhu, Y.; Xu, G.; Wang, R. C.; Chen, J.; Gao, W.; Zhu, T. L.; Shi, J. Y.; Fan, C. H.; Zhao, C. C.; Tian, H. Hydrogen Sulfide-Activatable Second Near-Infrared Fluorescent Nanoassemblies for Targeted Photothermal Cancer Therapy. *Nano Lett.* **2018**, *18*, 6411.
- (30) Wu, L.; Sun, Y.; Sugimoto, K.; Luo, Z.; Ishigaki, Y.; Pu, K.; Suzuki, T.; Chen, H.-Y.; Ye, D. Engineering of Electrochromic Materials as Activatable Probes for Molecular Imaging and Photodynamic Therapy. *J. Am. Chem. Soc.* **2018**, *140*, 16340.
- (31) Shi, B.; Ren, N.; Gu, L.; Xu, G.; Wang, R.; Zhu, T.; Zhu, Y.; Fan, C.; Zhao, C.; Tian, H. Theranostic Nanopatform with Hydrogen Sulfide Activatable NIR Responsiveness for Imaging-Guided On-Demand Drug Release. *Angew. Chem. Int. Ed.* **2019**, *58*, 16826.
- (32) Szabo, C.; Coletta, C.; Chao, C.; Módis, K.; Szczesny, B.; Papapetropoulos, A.; Hellmich, M. R. Tumor-derived hydrogen sulfide, produced by cystathionine-β-synthase, stimulates bioenergetics, cell proliferation, and angiogenesis in colon cancer. *Proc. Natl. Acad. Sci. U. S. A.* **2013**, *110*, 12474.
- (33) Lin, V. S.; Chen, W.; Xian, M.; Chang, C. J. Chemical probes for molecular imaging and detection of hydrogen sulfide and reactive sulfur species in biological systems. *Chem. Soc. Rev.* **2015**, *44*, 4596.
- (34) Hartle, M. D.; Pluth, M. D. A practical guide to working with H<sub>2</sub>S at the interface of chemistry and biology. *Chem. Soc. Rev.* **2016**, *45*, 6108.
- (35) Yi, L.; Xi, Z. Thiolysis of NBD-based dyes for colorimetric and fluorescence detection of H<sub>2</sub>S and biothiols: design and biological applications. *Org. Biomol. Chem.* **2017**, *15*, 3828.
- (36) Zhao, C.; Zhang, X.; Li, K.; Zhu, S.; Guo, Z.; Zhang, L.; Wang, F.; Fei, Q.; Luo, S.; Shi, P.; Tian, H.; Zhu, W.-H. Förster Resonance Energy Transfer Switchable Self-Assembled Micellar Nanoprobe: Ratiometric Fluorescent Trapping of Endogenous H<sub>2</sub>S Generation via Fluvastatin-Stimulated Upregulation. *J. Am. Chem. Soc.* **2015**, *137*, 8490.
- (37) Chen, W.; Pacheco, A.; Takano, Y.; Day, J. J.; Hanaoka, K.; Xian, M. A Single Fluorescent Probe to Visualize Hydrogen Sulfide and Hydrogen Polysulfides with Different Fluorescence Signals. *Angew. Chem. Int. Ed.* **2016**, *55*, 9993.
- (38) Lippert, A. R.; New, E. J.; Chang, C. J. Reaction-Based Fluorescent Probes for Selective Imaging of Hydrogen Sulfide in Living Cells. *J. Am. Chem. Soc.* **2011**, *133*, 10078.
- (39) Henthorn, H. A.; Pluth, M. D. Mechanistic Insights into the H<sub>2</sub>S-Mediated Reduction of Aryl Azides Commonly Used in H<sub>2</sub>S Detection. *J. Am. Chem. Soc.* **2015**, *137*, 15330.
- (40) Xu, G.; Guo, W.; Gu, X.; Wang, Z.; Wang, R.; Zhu, T.; Tian, H.; Zhao, C. Hydrogen Sulfide-Specific and NIR-Light-Controllable Synergistic Activation of Fluorescent Theranostic Prodrugs for Imaging-Guided Chemo-Photothermal Cancer Therapy. *CCS Chem.* **2020**, *2*, 527.
- (41) Sasakura, K.; Hanaoka, K.; Shibuya, N.; Mikami, Y.; Kimura, Y.; Komatsu, T.; Ueno, T.; Terai, T.; Kimura, H.; Nagano, T. Development of a Highly Selective Fluorescence Probe for Hydrogen Sulfide. *J. Am. Chem. Soc.* **2011**, *133*, 18003.
- (42) Shi, B.; Gu, X.; Fei, Q.; Zhao, C. Photoacoustic probes for real-time tracking of endogenous H<sub>2</sub>S in living mice. *Chem. Sci.* **2017**, *8*, 2150.
- (43) Wang, F.; Xu, G.; Gu, X.; Wang, Z.; Wang, Z.; Shi, B.; Lu, C.; Gong, X.; Zhao, C. Realizing highly chemoselective detection of H<sub>2</sub>S in vitro and in vivo with fluorescent probes inside core-shell silica nanoparticles. *Biomaterials* **2018**, *159*, 82.
- (44) Xu, G.; Yan, Q.; Lv, X.; Zhu, Y.; Xin, K.; Shi, B.; Wang, R.; Chen, J.; Gao, W.; Shi, P.; Fan, C.; Zhao, C.; Tian, H. Imaging of Colorectal Cancers Using Activatable Nanoprobes with Second Near-Infrared Window Emission. *Angew. Chem. Int. Ed.* **2018**, *57*, 3626.
- (45) Wang, R.; Dong, K.; Xu, G.; Shi, B.; Zhu, T.; Shi, P.; Guo, Z.; Zhu, W.-H.; Zhao, C. Activatable near-infrared emission-guided on-demand administration of photodynamic anticancer therapy with a theranostic nanoprobe. *Chem. Sci.* **2019**, *10*, 2785.
- (46) Shi, B.; Gu, X.; Wang, Z.; Xu, G.; Fei, Q.; Tang, J.; Zhao, C. Fine Regulation of Porous Architectures of Core-Shell Silica Nanocomposites Offers Robust Nanoprobes with Accelerated Responsiveness. *ACS Appl. Mater. Interfaces* **2017**, *9*, 35588.
- (47) Zhao, C. C.; Zhang, J. X.; Wang, X. Z.; Zhang, Y. F. Pyridone fused boron-dipyrromethenes: synthesis and properties. *Org. Biomol. Chem.* **2013**, *11*, 372.
- (48) Ye, D.; Shuhendler, A. J.; Cui, L.; Tong, L.; Tee, S. S.; Tikhomirov, G.; Felsher, D. W.; Rao, J. Bioorthogonal cyclization-mediated in situ self-assembly of small-molecule probes for imaging caspase activity in vivo. *Nat. Chem.* **2014**, *6*, 519.
- (49) Zhou, L.; Lv, F.; Liu, L.; Wang, S. In Situ-Induced Multivalent Anticancer Drug Clusters in Cancer Cells for Enhancing Drug Efficacy. *CCS Chem.* **2019**, *1*, 97.
- (50) Wu, Z.; Liang, D.; Tang, X. Visualizing Hydrogen Sulfide in Mitochondria and Lysosome of Living Cells and in Tumors of Living Mice with Positively Charged Fluorescent Chemosensors. *Anal. Chem.* **2016**, *88*, 9213.
- (51) Tian, H.; Qian, J.; Bai, H.; Sun, Q.; Zhang, L.; Zhang, W. Micelle-induced multiple performance improvement of fluorescent probes for H<sub>2</sub>S detection. *Anal. Chim. Acta* **2013**, *768*, 136.
- (52) Uchiyama, S.; Iwai, K.; de Silva, A. P. Multiplexing Sensory Molecules Map Protons Near Micellar Membranes. *Angew. Chem. Int. Ed.* **2008**, *47*, 4667.
- (53) Huang, J.; Li, J.; Lyu, Y.; Miao, Q.; Pu, K. Molecular optical imaging probes for early diagnosis of drug-induced acute kidney injury. *Nat. Mater.* **2019**, *18*, 1133.
- (54) Cheng, P.; Miao, Q.; Li, J.; Huang, J.; Xie, C.; Pu, K. Unimolecular Chemo-fluoro-luminescent Reporter for Crosstalk-Free Duplex Imaging of Hepatotoxicity. *J. Am. Chem. Soc.* **2019**, *141*, 10581.
- (55) Miao, Q.; Xie, C.; Zhen, X.; Lyu, Y.; Duan, H.; Liu, X.; Jøkerst, J. V.; Pu, K. Molecular afterglow imaging with bright, biodegradable polymer nanoparticles. *Nat. Biotech.* **2017**, *35*, 1102.

1 (56) Shao, A.; Xie, Y.; Zhu, S.; Guo, Z.; Zhu, S.; Guo, J.; Shi, P.;  
2 James, T. D.; Tian, H.; Zhu, W.-H. Far-Red and Near-IR AIE-Active  
3 Fluorescent Organic Nanoprobes with Enhanced Tumor-Targeting  
4 Efficacy: Shape-Specific Effects. *Angew. Chem. Int. Ed.* **2015**, *54*,  
5 7275.  
6  
7  
8  
9  
10  
11  
12  
13  
14  
15  
16  
17  
18  
19  
20  
21  
22  
23  
24  
25  
26  
27  
28  
29  
30  
31  
32  
33  
34  
35  
36  
37  
38  
39  
40  
41  
42  
43  
44  
45  
46  
47  
48  
49  
50  
51  
52  
53  
54  
55  
56  
57  
58  
59  
60

## SYNOPSIS TOC.

